Imaging-Based Quantum Tomography of Orbital-Angular-Momentum-Multiplexed Continuous-Variable Entangled States

Xiaolong Dong,[1,‡] Dongyu Liu,[1,2,‡] Mingsheng Tian,[1] Yi Li,[1] Shuheng Liu![ ],[1] Qiongyi He,[1,3,4]
Haitan Xu![ ],[5,6,7,*] and Zheng Li![ ][1,3,4,†]

[1]*State Key Laboratory for Mesoscopic Physics and Collaborative Innovation Center of Quantum Matter, School of Physics, Peking University, Beijing 10087, China*

[2]*Applied Physics Department, Stanford University, Stanford, California 94305, USA*

[3]*Collaborative Innovation Center of Extreme Optics, Shanxi University, Taiyuan, Shanxi 030006, China*

[4]*Peking University Yangtze Delta Institute of Optoelectronics, Nantong, Jiangsu 226010, China*

[5]*School of Materials Science and Intelligent Engineering, Nanjing University, Suzhou, Jiangsu 215163, China*

[6]*Shishan Laboratory, Nanjing University, Suzhou, Jiangsu 215163, China*

[7]*School of Physical Sciences, University of Science and Technology of China, Hefei, Anhui 230026, China*

Multiplexing techniques combine multiple signals into one channel, in order to increase the channel capacity and speed. Here we propose a correlation-based imaging method to efficiently measure the quantum states of orbital-angular-momentum (OAM)-multiplexed Gaussian light. The covariance matrices for all OAM components of the multiplexed Gaussian light can be efficiently reconstructed by one homodyne measurement on each beam. We also show that the proposed scheme can be simplified and implemented with only two charge coupled device detectors.

I. INTRODUCTION

Multiplexing has been a crucial technique in optical communication and processing technologies. One way to realize multiplexing in quantum information processing is to combine multiple degrees of freedom (DOF) of the light field, including time [1–4], wavelength [5,6], polarization [7,8], etc. Recent studies investigated continuous-variable (CV) quantum systems using orbital angular momentum (OAM) for multiplexing [9–11]. The OAM of light [12,13] was initially derived from the paraxial Helmholtz equation and characterizes the angular distribution of the light field, which has important applications in quantum information technology [14]. For discrete-variable quantum information processing, OAM was utilized in quantum teleportation with multiple DOFs of a single photon [15], generation of high-dimensional multiphoton entanglement [16], and entanglement swapping of multiple OAM states [17]. However, there have been few applications of OAM multiplexing in CV systems [18,19]. In this study, we propose a correlation imaging method [20] for the quantum tomography of OAM-multiplexed Gaussian light, which

can retrieve the quantum state represented by the covariance matrices [21,22] for all pairs of different OAMs in an OAM-multiplexed state using one homodyne measurement on each beam. We demonstrate this method by applying it to an OAM-multiplexed CV entanglement system that was recently realized in experiments [3,19]. Through nonlinear optical four-wave mixing [9], an entangled CV system containing two beams denoted as A and B can be deterministically generated [23–25], in which the two beams carry multiple pairs of entangled Laguerre-Gauss (LG) modes [26,27] $\text{LG}_{A,l}$ and $\text{LG}_{B,-l}$ [see Fig. 1(a)], where l is the topological charge corresponding to the OAM of the LG modes [9]. By spatially correlating the two light beams, we can efficiently deduce the covariance matrices $\sigma_{l,-l}$ of the amplitude and phase quadratures for each pair of the LG modes, which characterize the quantum state of the OAM-multiplexed Gaussian light.

II. THEORY

The OAM-multiplexed entangled CV states can be generated via techniques such as four-wave mixing as shown in Fig. 1(a), which corresponds to the following interaction Hamiltonian [9]:

$$\hat{H}_I = \sum_l i\hbar\gamma_l \hat{a}_l^\dagger \hat{b}_{-l}^\dagger + \text{h.c.}, \qquad (1)$$

*haitanxu@nju.edu.cn
†zheng.li@pku.edu.cn
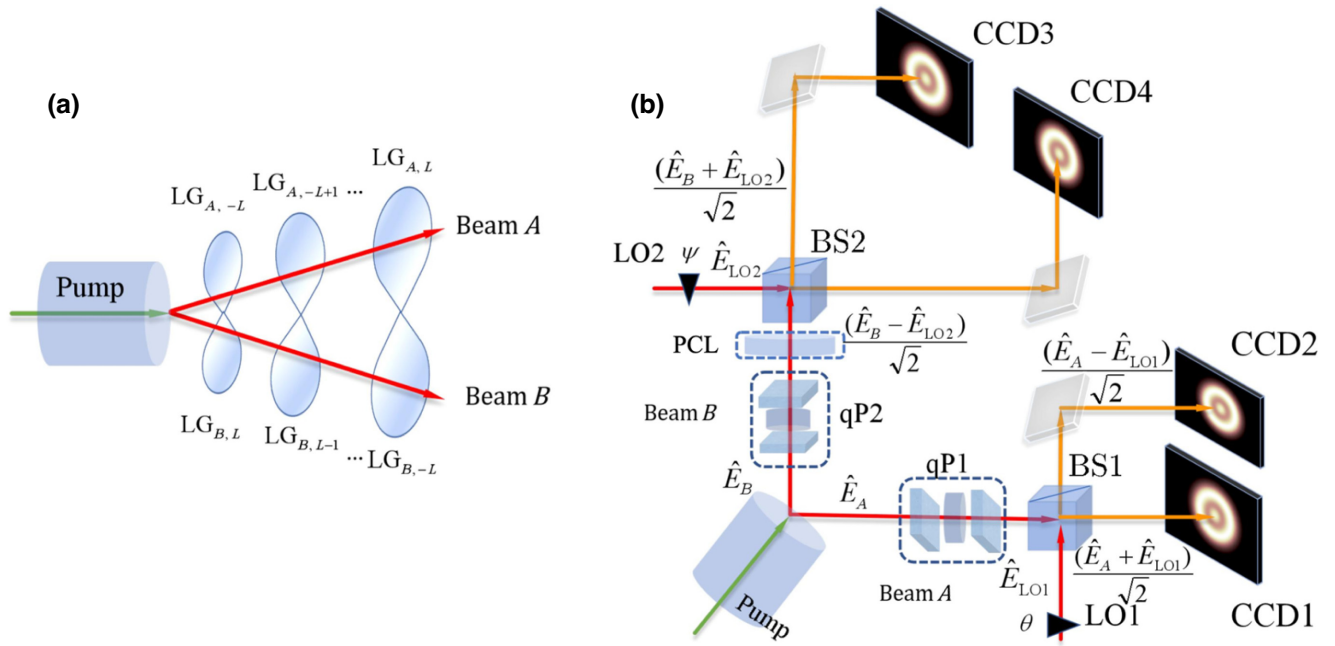‡These authors contributed equally to this work.

FIG. 1. (a) Illustration of an OAM-multiplexed CV entangled state. Two beams of light (beams *A* and *B*) are emitted from a pumped light source [9]. Both beams contain paired Gaussian modes $LG_{A,-l}$ and $LG_{B,l}$ with opposite topological charges $\pm l$, and each pair of OAM modes form a TMSS. (b) Schematic of the setup of the imaging-based detection system. BS, 50:50 beam splitter; LO, local oscillator; qP, *q*-plate, used for modifying the OAM of the light beams [28–30]; PCL, phase conjugate lens used to generate a forward phase conjugate wave. Each beam emitted from the light source is mixed with a coherent LO light with the same frequency by the beam splitter, with tunable phases θ and ϕ. After the mixing, the light fields are detected by the CCDs, which record the photocurrents on each pixel. Finally, the pixelwise photocurrents of the CCDs are processed to realize correlation measurement between CCD1 and CCD3 as well as CCD2 and CCD4.

where γ_l is the interaction strength between each pair of OAM modes and $\hat{a}_l^\dagger$, $\hat{b}_{-l}^\dagger$ are the creation operators associated with the different OAM LG modes in the two beams *A* and *B*, respectively. The resulting OAM-multiplexed state $|\Phi\rangle$ can be expressed as a direct product of two-mode squeezed states (TMSSs) with different l [3,9]:

$$|\Phi\rangle = S_{-L}|\text{vac}\rangle \otimes \cdots \otimes S_0|\text{vac}\rangle \otimes \cdots \otimes S_L|\text{vac}\rangle$$
$$= |\varphi\rangle_{-L} \otimes \cdots \otimes |\varphi\rangle_0 \otimes \cdots \otimes |\varphi\rangle_L, \quad (2)$$

where $S_l = e^{r_l(\hat{a}_l^\dagger \hat{b}_{-l}^\dagger - \hat{a}_l \hat{b}_{-l})}$ and $r_l = \gamma_l t$ is the squeezing parameter.

The light fields of Laguerre-Gauss modes are given by

$$u_l(r, \phi, z) = \sqrt{\frac{2}{\pi |l|!}} \sqrt{\frac{\hbar \omega}{\epsilon_0 V}} \frac{1}{w(z)} \left(\frac{r\sqrt{2}}{w(z)} \right)^{|l|}$$
$$\times \exp\left(-\frac{r^2}{w^2(z)} \right) \mathcal{L}_0^{|l|} \left(\frac{2r^2}{w^2(z)} \right)$$
$$\times \exp\left(-ik\frac{r^2}{2R(z)} \right) \exp(-il\phi) \exp(i\psi(z))$$
$$= E_l(r, z) \exp(-il\phi), \quad (3)$$

where w_0 is the radius of the beam waist, $w(z) = w_0\sqrt{1 + (z\lambda/\pi w_0^2 n)^2}$ is the radius of beam, and $R(z) = z[1 + (\pi w_0^2 n/z\lambda)^2]$ is the radius of curvature [31]. In our setup, the distance between pump light source and the CCD imaging planes is fixed, so we neglect the variable z in the following expressions except for Eq. (5).

The generation of the squeezed state $|\Phi\rangle$ is based on a nonlinear interaction Hamiltonian [9]:

$$\hat{H}(t) = \epsilon_0 \int d^3 r \chi^{(3)} \hat{E}_{p1}^*(\mathbf{r}, t) \hat{E}_{p2}^*(\mathbf{r}, t) \hat{E}_A(\mathbf{r}, t) \hat{E}_B(\mathbf{r}, t), \quad (4)$$

with $E_{p1,p2}$ being the pump fields. For convenience, let $E_{p1,p2}$ be plane waves, i.e., $E_{p1,p2} = E_{p1,p2}(r, z) \exp(-i\omega_{p1,p2}t) + \text{h.c.}$ After integrating over azimuthal angle ϕ, the Hamiltonian becomes

$$\hat{H}(t) = \epsilon_0 \int dz \int dr \chi^{(3)} \hat{E}_{p1}^* \hat{E}_{p2}^*$$
$$\times \sum_{l=-L}^{L} \hat{E}_l \hat{E}_{-l} e^{i(\omega_{p1}+\omega_{p2}-\omega_A-\omega_B)t} \hat{a}_l \hat{b}_{-l} + \text{h.c.} \quad (5)$$

Because of the energy and momentum conservation in the four-wave mixing process, only the terms of $\hat{a}_l \hat{b}_{-l}$ and

$\hat{a}_l^\dagger \hat{b}_{-l}^\dagger$ can survive in Eq. (5). This Hamiltonian indicates a squeezing process on each spatial mode l, so the form of states $|\Phi\rangle$ and the field operators are self-consistent. Due to the state being a direct product state, the field operator is the superposition of all different l. The electric field operators of the two beams in Fig. 1(a) can be expressed as

$$\hat{E}_A = \hat{E}_A^{(+)} + \hat{E}_A^{(-)}$$
$$= \sum_{l=-L}^{L} E_l(r_A) \exp(-il\phi - i\omega_A t)\hat{a}_l + \text{h.c.}, \quad (6)$$

$$\hat{E}_B = \hat{E}_B^{(+)} + \hat{E}_B^{(-)}$$
$$= \sum_{l=-L}^{L} E_{-l}(r_B) \exp(il\phi - i\omega_B t)\hat{b}_{-l} + \text{h.c.} \quad (7)$$

And the light intensity I_A reads

$$I_A(r_A, \phi_A) = \langle\Phi|\hat{E}_A^{(-)}\hat{E}_A^{(+)}|\Phi\rangle$$
$$= \sum_{l,l'=-L}^{L} E_l^*(r_A)E_{l'}(r_A)e^{-i(l'-l)\phi_A}\langle\Phi|\hat{a}_l^+\hat{a}_{l'}|\Phi\rangle,$$
$$(8)$$

where r_A and ϕ_A are coordinates on CCD1 and CCD2, and similarly for r_B and ϕ_B. We integrate light intensities over azimuthal angle ϕ:

$$\mathcal{I}_i(r_i) = \int_0^{2\pi} I_i d\phi_i = 2\pi \sum_{l=-L}^{L} I_{i,l}, \quad (9)$$

where $I_{i,l} = E_l^*(r)E_l(r)\langle n_{i,l}\rangle$ and $i = A, B$. Because LG modes have the property that $E_l(r) = E_{-l}(r)$, generally $\langle n_{i,l}\rangle$ cannot be distinguished from $\langle n_{i,-l}\rangle$.

To distinguish the $\langle n_{i,\pm l}\rangle$ components from each other, we use q-plates to modify both the OAM topological charges and radial distribution of the two light beams. After the q-plate operations, the OAM topological charges are modified as $\Delta l_A = 1$, $\Delta l_B = -1$. The q-plate [see Fig. 1(b)] consists of a thin birefringent liquid crystal sandwiched between containing glasses, whose optic axis is structured for the pattern with topological charge q, which can impart the corresponding OAM topological charge to the light modes [28,29].

When a beam is transmitted through a q-plate, the radial distribution of each mode is reshaped into a hypergeometric-Gaussian (HyGG) form [32,33]. When the topological charges of the two beams are modified by $\Delta l_A = 1$ and $\Delta l_B = -1$, respectively, the amplitude

distributions of the output modes are expressed as

$$E_{l_A+1,A}^{\text{out}}(r,z) = \text{HyGG}_{|l_A|-\mu_A(l_A),\mu_A(l_A)}(r,z),$$
$$E_{l_B-1,B}^{\text{out}}(r,z) = \text{HyGG}_{|l_B|-\mu_B(l_B),\mu_B(l_B)}(r,z), \quad (10)$$

where $\mu_A(l_A) = \sqrt{(l_A + 1/2)^2 + (1/2)^2}$, $\mu_B(l_B) = \sqrt{(l_B - 1/2)^2 + (-1/2)^2}$, l_A and l_B are the OAM quantum numbers of the input modes of beams A and B, and the HyGG function is

$$\text{HyGG}_{p,m}(\rho, \zeta)$$
$$= C_{p,m}\zeta^{p/2}(\zeta + i)^{-(1+|m|+p/2)}\rho^{|m|}e^{-i\rho^2/(\zeta+i)}{}_1$$
$$\times F_1\left(-\frac{p}{2}, 1 + |m|; \frac{\rho^2}{\zeta(\zeta+i)}\right), \quad (11)$$

where $C_{p,m} = i^{|m|+1}\sqrt{2^{p+|m|+1}/\pi\,\Gamma(p+|m|+1)}\Gamma(1 + |m| + p/2)/\Gamma(|m|+1)$, ${}_1F_1$ is the confluent hypergeometric function of the first kind, $\rho = r/w_0$, and $\zeta = z/(k_0 w_0^2/2)$.

We can reexpress Eq. (9) for beams A and B after the $\Delta l_A = 1$ and $\Delta l_B = -1$ operations as

$$\mathcal{I}'_A(r) = 2\pi \sum_{l_A=-L}^{L} |E_{l_A+1,A}^{\text{out}}(r)|^2\langle n_{A,l_A},\rangle$$
$$\mathcal{I}'_B(r) = 2\pi \sum_{l_B=-L}^{L} |E_{l_B-1,B}^{\text{out}}(r)|^2\langle n_{B,l_B}\rangle. \quad (12)$$

As $|E_{l,A}^{\text{out}}(r)|^2$'s for all l are linearly independent of each other after the q-plate operation and the same for $|E_{l,B}^{\text{out}}(r)|^2$'s, we can obtain the values of all $\langle n_{A,l}\rangle$ and $\langle n_{B,l}\rangle$ by fitting the radial distribution of each beam after the q-plate with Eq. (12).

The covariance matrix of the OAM-resolved TMSS consisting of $\text{LG}_{A,l}$ and $\text{LG}_{B,-l}$ uniquely characterizes the multiplexed Gaussian states. Consider the generic form of the Gaussian state covariance matrix [34]:

$$\sigma_{l,-l} = \langle X_{i,l}X_{j,l} + X_{j,l}X_{i,l}\rangle = \begin{pmatrix} \mathcal{A}_1 & 0 & \mathcal{C}_1 & \mathcal{D}_2 \\ 0 & \mathcal{A}_1 & \mathcal{D}_1 & \mathcal{C}_2 \\ \mathcal{C}_1 & \mathcal{D}_1 & \mathcal{B}_1 & 0 \\ \mathcal{D}_2 & \mathcal{C}_2 & 0 & \mathcal{B}_1 \end{pmatrix}, \quad (13)$$

where $X_{i,l} \in \{x_{i,l} - \langle x_{i,l}\rangle, p_{i,l} - \langle p_{i,l}\rangle\}$, $i,j = A,B$. The first-order moments $\langle x_{i,l}\rangle$ and $\langle p_{i,l}\rangle$ of the $\text{LG}_{i,\pm l}$ modes of the two beams can be set to zero by a simple translation operation, without changing other properties. So $\mathcal{A}_1 = \langle 2n_{A,l} + 1\rangle$, $\mathcal{B}_1 = \langle 2n_{B,-l} + 1\rangle$, $\mathcal{C}_1 = \langle x_{A,l}x_{B,-l}\rangle$, $\mathcal{C}_2 = \langle p_{A,l}p_{B,-l}\rangle$, $\mathcal{D}_2 = \langle x_{A,l}p_{B,-l}\rangle$, and $\mathcal{D}_1 = \langle p_{A,l}x_{B,-l}\rangle$, where $x_{i,l}$ and $p_{i,l}$ are the phase-amplitude quadratures of the mode $\text{LG}_{i,l}$ in the CV states. $\mathcal{A}_1$ and $\mathcal{B}_1$ can be immediately obtained from first-order intensities $\mathcal{I}_i(r)$ by using Eqs. (9)–(12). To retrieve the off-diagonal elements of the covariance

matrix, we use two local oscillators (LO1 and LO2), the field operators of which are simple Gaussian wavepackets:

$$\hat{E}_{\text{LO1}} = \hat{E}_{\text{LO1}}^{(+)} + \hat{E}_{\text{LO1}}^{(-)} = E_{\text{LO1}} \exp(-i\omega_A t)\hat{c}_1 + \text{h.c.,} \quad (14)$$

$$\hat{E}_{\text{LO2}} = \hat{E}_{\text{LO2}}^{(+)} + \hat{E}_{\text{LO2}}^{(-)} = E_{\text{LO2}} \exp(-i\omega_B t)\hat{c}_2 + \text{h.c.,} \quad (15)$$

where E_{LO1} and E_{LO2} carry tunable phases θ and ψ, respectively [see Fig. 1(b)]. Both LO beams have the same frequency as the beams A and B, similar to homodyne detection. In order to calibrate the phase θ, we can use the fact that when $\theta = 0$, the intensity on CCD1 will be

maximum and intensity on CCD2 will be minimum, and similarly for ψ. For strong coherent LO beams, the coherent states are denoted as $|\alpha\rangle$ and $|\beta\rangle$. The usual approximations $\hat{c}_1^\dagger|\alpha\rangle \simeq \alpha^*|\alpha\rangle$ and $\hat{c}_2^\dagger|\beta\rangle \simeq \beta^*|\beta\rangle$ are taken for strong LO beams.

After beam mixing by the BS, the field operators become $\hat{E}_{1,2} = \frac{1}{\sqrt{2}}(\hat{E}_A \pm \hat{E}_{\text{LO1}})$ and $\hat{E}_{3,4} = \frac{1}{\sqrt{2}}(\hat{E}_B \pm \hat{E}_{\text{LO2}})$. The corresponding second-order intensity functions for the mixed signals measured by CCD1 and CCD3 (denoted as $I_+^{(2)}$) as well as by CCD2 and CCD4 (denoted as $I_-^{(2)}$) are given by

$$I_\pm^{(2)}(r,\phi) = \begin{cases} \langle \hat{E}_1^{(-)}\hat{E}_3^{(-)}\hat{E}_3^{(+)}\hat{E}_1^{(+)} \rangle \\ \langle \hat{E}_2^{(-)}\hat{E}_4^{(-)}\hat{E}_4^{(+)}\hat{E}_2^{(+)} \rangle \end{cases} = \frac{1}{4}(I_0^{(2)} + I_A|E_{\text{LO2}}|^2\langle n_{\text{LO2}}\rangle + I_B|E_{\text{LO1}}|^2\langle n_{\text{LO1}}\rangle + \langle n_{\text{LO1}}\rangle\langle n_{\text{LO2}}\rangle|E_{\text{LO1}}|^2|E_{\text{LO2}}|^2 \pm \xi)$$

$$+ \frac{1}{4}\left[\sum_{l_1,l_2=-L}^{L} \langle (E_{l_1}^*(r)e^{il_1\phi}\hat{a}_{l_1}^\dagger E_{\text{LO1}}\hat{c}_1 + E_{l_1}(r)e^{-il_1\phi}\hat{a}_{l_1}E_{\text{LO1}}^*\hat{c}_1^\dagger) \right.$$

$$\left. \times (E_{l_2}^*(r)e^{-il_2\phi}\hat{b}_{l_2}^\dagger E_{\text{LO2}}\hat{c}_2 + E_{l_2}(r)e^{il_2\phi}\hat{b}_{l_2}E_{\text{LO2}}^*\hat{c}_2^\dagger) \rangle \right], \quad (16)$$

and with the additional phase conjugate operation on beam B as shown in Fig. 1(b), we can obtain

$$I_{\text{conj}\pm}^{(2)}(r,\phi) = \begin{cases} \langle \hat{E}_1^{(-)}\hat{E}_3^{(-)}\hat{E}_3^{(+)}\hat{E}_1^{(+)} \rangle \\ \langle \hat{E}_2^{(-)}\hat{E}_4^{(-)}\hat{E}_4^{(+)}\hat{E}_2^{(+)} \rangle \end{cases} = \frac{1}{4}(I_0^{(2)} + I_A|E_{\text{LO2}}|^2\langle n_{\text{LO2}}\rangle + I_B|E_{\text{LO1}}|^2\langle n_{\text{LO1}}\rangle + \langle n_{\text{LO1}}\rangle\langle n_{\text{LO2}}\rangle|E_{\text{LO1}}|^2|E_{\text{LO2}}|^2 \pm \xi')$$

$$+ \frac{1}{4}\left[\sum_{l_1,l_2=-L}^{L} \langle (E_{l_1}^*(r)e^{il_1\phi}\hat{a}_{l_1}^\dagger E_{\text{LO1}}\hat{c}_1 + E_{l_1}(r)e^{-il_1\phi}\hat{a}_{l_1}E_{\text{LO1}}^*\hat{c}_1^\dagger) \right.$$

$$\left. \times (E_{l_2}(r)e^{il_2\phi}\hat{b}_{l_2}^\dagger E_{\text{LO2}}\hat{c}_2 + E_{l_2}^*(r)e^{-il_2\phi}\hat{b}_{l_2}E_{\text{LO2}}^*\hat{c}_2^\dagger) \rangle \right], \quad (17)$$

where $I_0^{(2)}(r_A, r_B, \phi_A, \phi_B) = \langle \hat{E}_A^{(-)}\hat{E}_B^{(-)}\hat{E}_B^{(+)}\hat{E}_A^{(+)} \rangle$ is independent of the LO beams, and ξ and ξ' denote the terms that will be cancelled out when the second-order intensity functions are added up.

Integrating over the azimuthal angle, and applying the approximations for strong coherent LO beams to the operators $\hat{c}_{1,2}$, the summation of the second-order intensity functions becomes

$$\mathcal{I}_{\text{sum}}^{(2)}(r) = \int_0^{2\pi} d\phi (I_+^{(2)} + I_-^{(2)} + I_{\text{conj}+}^{(2)} + I_{\text{conj}-}^{(2)})$$

$$= \mathcal{I}_0^{(2)} + \mathcal{I}_A|E_{\text{LO2}}|^2\langle n_{\text{LO2}}\rangle + \mathcal{I}_B|E_{\text{LO1}}|^2\langle n_{\text{LO1}}\rangle + 2\pi\langle n_{\text{LO1}}\rangle\langle n_{\text{LO2}}\rangle|E_{\text{LO1}}|^2|E_{\text{LO2}}|^2$$

$$+ \pi\mathcal{E}\sum_{l=-L}^{L}|E_l(r)|^2\langle(\hat{a}_l e^{i\theta} + \hat{a}_l^\dagger e^{-i\theta})(\hat{b}_{-l}e^{i\psi} + \hat{b}_{-l}^\dagger e^{-i\psi})\rangle, \quad (18)$$

where $\mathcal{I}_0^{(2)} = \int_0^{2\pi} I_0^{(2)} d\phi$, $\mathcal{E} = |E_{\text{LO1}}E_{\text{LO2}}\alpha\beta|$, and the phases θ and ψ are tunable.
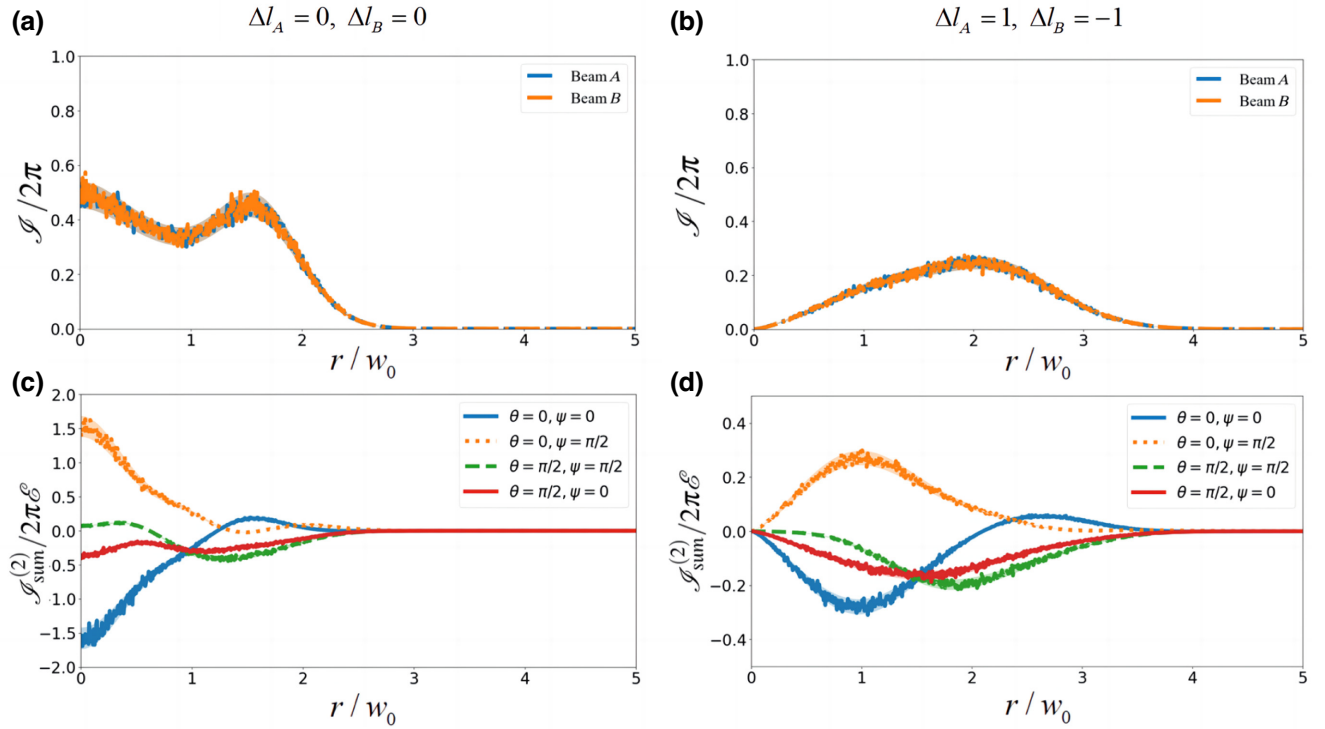
FIG. 2. Simulated first- and second-order intensity signals for the measurement of OAM-multiplexed CV states. (a),(c) The first-order intensity $\mathcal{I}(r)$ and the second-order intensity $\mathcal{I}_{sum}^{(2)}(r)$ without the q-plates. (b),(d) The intensity signals with the topological charge of the beams modified by the q-plate. In (c),(d), the phases of the local oscillators θ and ψ are adjusted to retrieve the off-diagonal elements of covariance matrices $\boldsymbol{\sigma}_{l,-l}$. In the simulation, Gaussian noises are added to the signals, resulting in measurement uncertainty represented by the shaded areas.

Setting (θ, ψ) to $(0,0)$, $(0, \pi/2)$, $(\pi/2, 0)$, or $(\pi/2, \pi/2)$, we have

$$\langle(\hat{a}_l e^{i\theta} + \hat{a}_l^\dagger e^{-i\theta})(\hat{b}_{-l} e^{i\psi} + \hat{b}_{-l}^\dagger e^{-i\psi})\rangle = \begin{cases} \langle x_{A,l} x_{B,-l} \rangle = \mathcal{C}_1, & (\theta, \psi) = (0,0), \\ \langle x_{A,l} p_{B,-l} \rangle = \mathcal{D}_2, & (\theta, \psi) = (0, \pi/2), \\ \langle p_{A,l} x_{B,-l} \rangle = \mathcal{D}_1, & (\theta, \psi) = (\pi/2, 0), \\ \langle p_{A,l} p_{B,-l} \rangle = \mathcal{C}_2, & (\theta, \psi) = (\pi/2, \pi/2). \end{cases} \qquad (19)$$
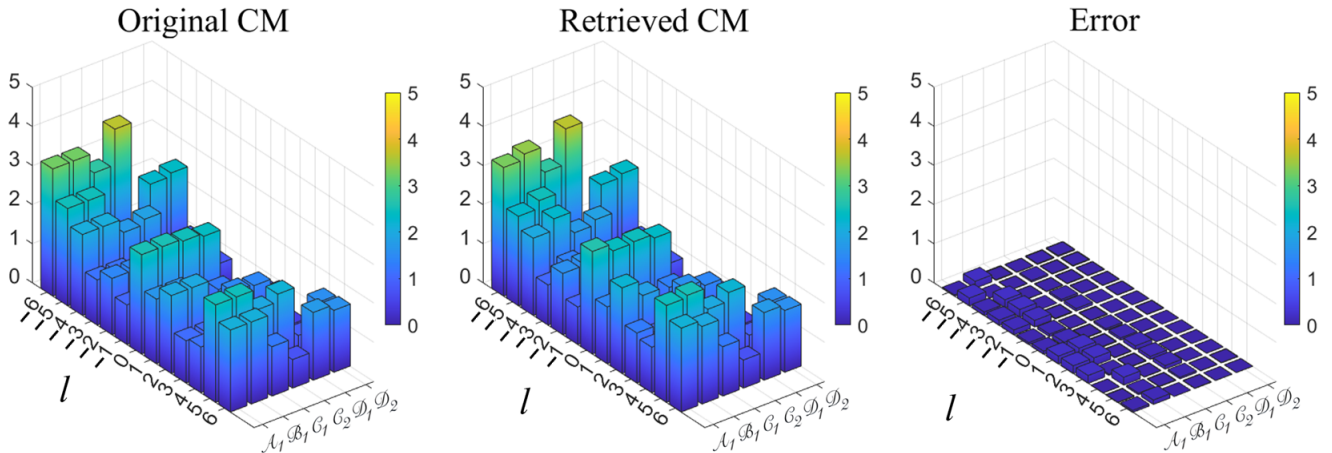

FIG. 3. The original and retrieved covariance matrix (CM) elements of an arbitrarily chosen OAM-multiplexed Gaussian CV entangled state, and the absolute error of the retrieved covariance matrices $\boldsymbol{\sigma}_{l,-l}$.
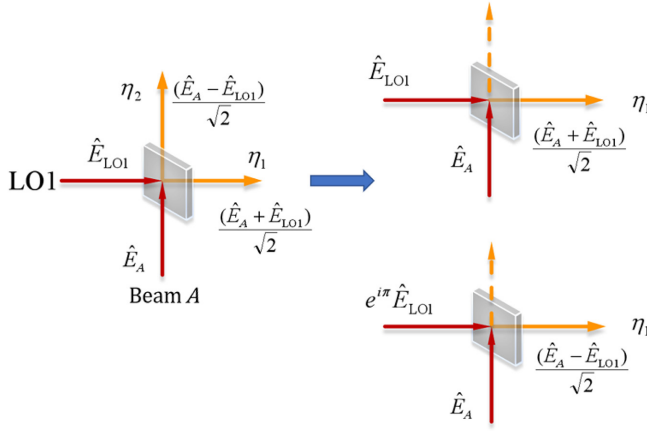
FIG. 4. Treatment of imperfect quantum efficiencies of the imaging system, with a simplified measurement scheme using only two CCDs. By adjusting the relative phase of the local oscillator LO1 from θ to $\theta + \pi$, we can get both $I^{(2)}_\pm$ with CCD1 and CCD3.

Similar to the treatment of the first-order intensity functions, we can apply q-plate operations to the second-order correlation functions. As $E^{\text{out}}_{l+1,A}(r) = E^{\text{out}}_{-l-1,B}(r)$, we can denote $E^{\text{out}}_{l+1,A}(r)$ and $E^{\text{out}}_{-l-1,B}(r)$ simply by $E^{\text{out}}_{l+1}(r)$. $\mathcal{I}^{(2)}_{\text{sum}}(r)$ after the q-plate operations becomes

$$
\begin{aligned}
\mathcal{I}^{(2)\prime}_{\text{sum}}(r) = {}& \mathcal{I}^{(2)\prime}_0 + \mathcal{I}'_A |E_{\text{LO2}}|^2 \langle n_{\text{LO2}} \rangle + \mathcal{I}'_B |E_{\text{LO1}}|^2 \langle n_{\text{LO1}} \rangle \\
& + 2\pi \langle n_{\text{LO1}} \rangle \langle n_{\text{LO2}} \rangle |E_{\text{LO1}}|^2 |E_{\text{LO2}}|^2 \\
& + \pi \mathcal{E} \sum_{l=-L}^{L} |E^{\text{out}}_{l+1}(r)|^2 \langle (\hat{a}_l e^{i\theta} + \hat{a}^\dagger_l e^{-i\theta}) \\
& \times (\hat{b}_{-l} e^{i\psi} + \hat{b}^\dagger_{-l} e^{-i\psi}) \rangle.
\end{aligned}
\tag{20}
$$

For each set of (θ, ψ), we have a correlation intensity curve $\mathcal{I}^{(2)\prime}_{\text{sum}}(r)$. As $E^{\text{out}}_{l+1}(r)$'s are linearly independent of each other, by fitting the data shown in Figs. 2(b) and 2(d) with Eq. (20), we can obtain $\langle q_{A,l} q_{B,-l} \rangle$ for $l = -L, -L + 1, \ldots, L$, where q denotes x or p. The off-diagonal elements of the OAM-resolved covariance matrix $\boldsymbol{\sigma}_{l,-l}$ can thus be obtained.

III. RESULTS AND DISCUSSION

We simulate the summed second-order correlation intensity $\mathcal{I}^{(2)}_{\text{sum}}(r)$ and first-order intensity $\mathcal{I}(r)$ for an OAM-multiplexed state composed of two-mode squeezed states of multiple l and present $\mathcal{I}^{(2)}_{\text{sum}}(r)$ and $\mathcal{I}(r)$ in Fig. 2. In realistic experiments, there could be noises resulting in uncertainty in the measured signals. We add Gaussian noises with a variance of $\sigma = 0.05$ to the simulated intensity signals to represent the noises in real experiments, which are shown by the shaded areas in Fig. 2. We then demonstrate the reconstruction of the covariance matrices in the presence of noises in the signals, and fully determine the quantum states of the OAM-multiplexed Gaussian CV entangled light. For the covariance matrix $\sigma_{l,-l}$ of every OAM block of the multiplexed state, the diagonal terms $\mathcal{A}_1$ and $\mathcal{B}_1$ are obtained by fitting the first-order intensities $\mathcal{I}(r)$ in Fig. 2(b) with Eq. (12), and the off-diagonal terms $\mathcal{C}_{1,2}$ and $\mathcal{D}_{1,2}$ are obtained from the second-order correlation intensities $\mathcal{I}^{(2)}_{\text{sum}}(r)$ in Fig. 2(d) with Eqs. (19) and (20). The original and retrieved covariance matrices of the two multiplexed CV states are presented in Fig. 3.

In real experiments, the quantum efficiency of the imaging system is not perfect, especially for the CCD detectors. We investigate the effect of imperfect quantum efficiency by adding attenuation factors η_1 to η_3 to the detectors CCD1 and CCD3. Because the field operators of the two mixed output modes can be exchanged by adjusting the phases of the corresponding local oscillators from θ to $\theta + \pi$, as shown in Fig. 4(a), we can simplify the experimental setup with only two CCDs, i.e., we can measure $I^{(2)}_+(r)$ by setting the phase of LO1 to θ, and $I^{(2)}_-(r)$ by changing the phase of LO1 to $\theta + \pi$, similarly for $I^{(2)}_{\text{conj}\pm}(r)$.

The imperfect quantum efficiency results in a transformation $\hat{a} \longrightarrow \sqrt{\eta}\hat{a}$ when the operators are normally ordered, and similarly for the $\hat{a}^\dagger$ operator [35]. Thus the first-order intensities should be multiplied by η_1 or η_3, and similarly for the retrieved $\langle n_l \rangle$. On the other hand, the second-order intensity functions of the two beams should be multiplied by $\eta_1 \eta_3$. As a result, $I^{(2)}_{\text{sum}}(r)$ in Eq. (18) becomes

$$
\begin{aligned}
\mathcal{I}^{(2)}_{\text{sum}}(r) = {}& \eta_1 \eta_3 (\mathcal{I}^{(2)}_0 + \mathcal{I}_A |E_{\text{LO2}}|^2 \langle n_{\text{LO2}} \rangle + \mathcal{I}_B |E_{\text{LO1}}|^2 \langle n_{\text{LO1}} \rangle) + \langle n_{\text{LO1}} \rangle \langle n_{\text{LO2}} \rangle |E_{\text{LO1}}|^2 |E_{\text{LO2}}|^2 \\
& + \pi \mathcal{E} \sum_{l=-L}^{L} |E_l(r)|^2 \sqrt{\eta_1 \eta_3} \langle \sqrt{\eta_1 \eta_3} (\hat{a}_l e^{i\theta} + \hat{a}^\dagger_l e^{-i\theta})(\hat{b}_{-l} e^{i\psi} + \hat{b}^\dagger_{-l} e^{-i\psi}) \rangle,
\end{aligned}
\tag{21}
$$

and the result after q-plate operations changes similarly. Thus, the measured OAM-resolved covariance matrix $\boldsymbol{\sigma}_{l,-l}$ becomes

$$\boldsymbol{\sigma}_{l,-l}(\eta_1, \eta_3) = \begin{pmatrix} (\mathcal{A}_1 - 1)\eta_1 + 1 & 0 & \sqrt{\eta_1\eta_3}\mathcal{C}_1 & \sqrt{\eta_1\eta_3}\mathcal{D}_2 \\ 0 & (\mathcal{A}_1 - 1)\eta_1 + 1 & \sqrt{\eta_1\eta_3}\mathcal{D}_1 & \sqrt{\eta_1\eta_3}\mathcal{C}_2 \\ \sqrt{\eta_1\eta_3}\mathcal{C}_1 & \sqrt{\eta_1\eta_3}\mathcal{D}_1 & (\mathcal{B}_1 - 1)\eta_3 + 1 & 0 \\ \sqrt{\eta_1\eta_3}\mathcal{D}_2 & \sqrt{\eta_1\eta_3}\mathcal{C}_2 & 0 & (\mathcal{B}_1 - 1)\eta_3 + 1 \end{pmatrix}. \tag{22}$$

The original covariance matrices can therefore be recovered by using only two CCDs and rescaling with η_1 and η_3.

IV. CONCLUSION

In conclusion, we propose a method to quantum tomographically retrieve OAM-multiplexed Gaussian CV entangled states using a correlation imaging technique. Taking advantage of the spatial resolution power of the imaging system, we need to perform only a small set of measurements, and can potentially speed up the OAM-multiplexed quantum information processing and measurement. Furthermore, the application of our method is not limited to specific spatial distribution of the light modes, such as Laguerre-Gaussian and hypergeometric-Gaussian distributions. With the output radial distribution of the OAM modes, we can use this method to retrieve the covariance matrix of the corresponding OAM-multiplexed state.

ACKNOWLEDGMENTS

[1] Shota Yokoyama, Ryuji Ukai, Seiji C. Armstrong, Chanond Sornphiphatphong, Toshiyuki Kaji, Shigenari Suzuki, Jun-Ichi Yoshikawa, Hidehiro Yonezawa, Nicolas C. Menicucci, and Akira Furusawa, Ultra-large-scale continuous-variable cluster states multiplexed in the time domain, Nat. Photonics **7**, 982 (2013).

[2] Alireza Marandi, Zhe Wang, Kenta Takata, Robert L. Byer, and Yoshihisa Yamamoto, Network of time-multiplexed optical parametric oscillators as a coherent Ising machine, Nat. Photonics **8**, 937 (2014).

[3] Rajveer Nehra, Ryoto Sekine, Luis Ledezma, Qiushi Guo, Robert M. Gray, Arkadev Roy, and Alireza Marandi, Few-cycle vacuum squeezing in nanophotonics, Science **377**, 1333 (2022).

[4] Warit Asavanant, Yu Shiozawa, Shota Yokoyama, Baramee Charoensombutamon, Hiroki Emura, Rafael N. Alexander, Shuntaro Takeda, Jun I. Yoshikawa, Nicolas C. Menicucci, Hidehiro Yonezawa, and Akira Furusawa, Generation of time-domain-multiplexed two-dimensional cluster state, Science **366**, 373 (2019).

[5] F. A. S. Barbosa, Antonio Sales Coelho, L. F. Muñoz-Martínez, L. Ortiz-Gutiérrez, A. S. Villar, P. Nussenzveig, and M. Martinelli, Hexapartite Entanglement in an Above-Threshold Optical Parametric Oscillator, Phys. Rev. Lett. **121**, 073601 (2018).

[6] M. Grimau Puigibert, G. H. Aguilar, Q. Zhou, F. Marsili, M. D. Shaw, V. B. Verma, S. W. Nam, D. Oblak, and W. Tittel, Heralded Single Photons Based on Spectral Multiplexing and Feed-Forward Control, Phys. Rev. Lett. **119**, 083601 (2017).

[7] Deny R. Hamel, Lynden K. Shalm, Hannes Hübel, Aaron J. Miller, Francesco Marsili, Varun B. Verma, Richard P. Mirin, Sae W. Nam, Kevin J. Resch, and Thomas Jennewein, Direct generation of three-photon polarization entanglement, Nat. Photonics **8**, 801 (2014).

[8] Hongwei Liu, Jipeng Wang, Haiqiang Ma, and Shihai Sun, Polarization-multiplexing-based measurement-device-independent quantum key distribution without phase reference calibration, Optica **5**, 902 (2018).

[9] Xiaozhou Pan, Sheng Yu, Yanfen Zhou, Kun Zhang, Kai Zhang, Shuchao Lv, Sijin Li, Wei Wang, and Jietai Jing, Orbital-Angular-Momentum Multiplexed Continuous-Variable Entanglement from Four-Wave Mixing in Hot Atomic Vapor, Phys. Rev. Lett. **123**, 070506 (2019).

[10] Yingxuan Chen, Shengshuai Liu, Yanbo Lou, and Jietai Jing, Orbital Angular Momentum Multiplexed Quantum Dense Coding, Phys. Rev. Lett. **127**, 093601 (2021).

[11] Kai Zhang, Wei Wang, Shengshuai Liu, Xiaozhou Pan, Jinjian Du, Yanbo Lou, Sheng Yu, Shuchao Lv, Nicolas Treps, and Claude Fabre, *et al.*, Reconfigurable Hexapartite Entanglement by Spatially Multiplexed Four-Wave Mixing Processes, Phys. Rev. Lett. **124**, 090501 (2020).

[12] Robert Fickler, Radek Lapkiewicz, William N. Plick, Mario Krenn, Christoph Schaeff, Sven Ramelow, and Anton Zeilinger, Quantum entanglement of high angular momenta, Science **338**, 640 (2012).

[13] L. Allen, M. W. Beijersbergen, R. J. C. Spreeuw, and J. P. Woerdman, Orbital angular momentum of light and the transformation of Laguerre-Gaussian laser modes, Phys. Rev. A **45**, 8185 (1992).

[14] Robert Fickler, Radek Lapkiewicz, Marcus Huber, Martin P. J. Lavery, Miles J. Padgett, and Anton Zeilinger, Interface between path and orbital angular momentum entanglement for high-dimensional photonic quantum information, Nat. Commun. **5**, 1 (2014).

[15] Xi-Lin Wang, Xin-Dong Cai, Zu-En Su, Ming-Cheng Chen, Dian Wu, Li Li, Nai-Le Liu, Chao-Yang Lu, and

Jian-Wei Pan, Quantum teleportation of multiple degrees of freedom of a single photon, Nature **518**, 516 (2015).

[16] Wei Zhang, Dong-Sheng Ding, Ming-Xin Dong, Shuai Shi, Kai Wang, Shi-Long Liu, Yan Li, Zhi-Yuan Zhou, Bao-Sen Shi, and Guang-Can Guo, Experimental realization of entanglement in multiple degrees of freedom between two quantum memories, Nat. Commun. **7**, 1 (2016).

[17] Yingwen Zhang, Megan Agnew, Thomas Roger, Filippus S. Roux, Thomas Konrad, Daniele Faccio, Jonathan Leach, and Andrew Forbes, Simultaneous entanglement swapping of multiple orbital angular momentum states of light, Nat. Commun. **8**, 1 (2017).

[18] M. Lassen, G. Leuchs, and U. L. Andersen, Continuous Variable Entanglement and Squeezing of Orbital Angular Momentum States, Phys. Rev. Lett. **102**, 163602 (2009).

[19] A. M. Marino, V. Boyer, R. C. Pooser, P. D. Lett, K. Lemons, and K. M. Jones, Delocalized Correlations in Twin Light Beams with Orbital Angular Momentum, Phys. Rev. Lett. **101**, 093602 (2008).

[20] Da Zhang, Yan-Hua Zhai, Ling-An Wu, and Xi-Hao Chen, Correlated two-photon imaging with true thermal light, Opt. Lett. **30**, 2354 (2005).

[21] Gerardo Adesso and Fabrizio Illuminati, Gaussian measures of entanglement versus negativities: Ordering of two-mode Gaussian states, Phys. Rev. A **72**, 032334 (2005).

[22] Joel F. Corney and Peter D. Drummond, Gaussian quantum operator representation for bosons, Phys. Rev. A **68**, 063822 (2003).

[23] Mikkel V. Larsen, Xueshi Guo, Casper R. Breum, Jonas S. Neergaard-Nielsen, and Ulrik L. Andersen, Deterministic generation of a two-dimensional cluster state, Science **366**, 369 (2019).

[24] Moran Chen, Nicolas C. Menicucci, and Olivier Pfister, Experimental Realization of Multipartite Entanglement of 60 Modes of a Quantum Optical Frequency Comb, Phys. Rev. Lett. **112**, 120505 (2014).

[25] Wei Liu, Rong Ma, Li Zeng, Zhongzhong Qin, and Xiaolong Su, Quantum beam splitter for orbital angular momentum of light: Quantum correlation by four-wave mixing operated in a nonamplifying regime, Opt. Lett. **44**, 2053 (2019).

[26] Francesco Pampaloni and Jörg Enderlein, Gaussian, Hermite-Gaussian, and Laguerre-Gaussian beams: A primer, ArXiv:physics/0410021 (2004).

[27] Dunzhao Wei, Yue Cheng, Rui Ni, Yong Zhang, Xiaopeng Hu, Shining Zhu, and Min Xiao, Generating Controllable Laguerre-Gaussian Laser Modes Through Intracavity Spin-Orbital Angular Momentum Conversion of Light, Phys. Rev. Appl. **11**, 014038 (2019).

[28] L. Marrucci, C. Manzo, and D. Paparo, Optical Spin-to-Orbital Angular Momentum Conversion in Inhomogeneous Anisotropic Media, Phys. Rev. Lett. **96**, 163905 (2006).

[29] A. Pecoraro, F. Cardano, L. Marrucci, and A. Porzio, Continuous-variable entangled states of light carrying orbital angular momentum, Phys. Rev. A **100**, 012321 (2019).

[30] Fang-Xiang Wang, Wei Chen, Zhen-Qiang Yin, Shuang Wang, Guang-Can Guo, and Zheng-Fu Han, Characterizing High-Quality High-Dimensional Quantum Key Distribution by State Mapping Between Different Degrees of Freedom, Phys. Rev. Appl. **11**, 024070 (2019).

[31] Orazio Svelto and David C. Hanna, *Principles of Lasers* (Springer, New York, 1998), Vol. 4.

[32] Ebrahim Karimi, Gianluigi Zito, Bruno Piccirillo, Lorenzo Marrucci, and Enrico Santamato, Hypergeometric-Gaussian modes, Opt. Lett. **32**, 3053 (2007).

[33] Ebrahim Karimi, Bruno Piccirillo, Lorenzo Marrucci, and Enrico Santamato, Light propagation in a birefringent plate with topological charge, Opt. Lett. **34**, 1225 (2009).

[34] Alessio Serafini, *Quantum Continuous Variables: A Primer Of Theoretical Methods* (CRC Press, Florida, London, New York, 2017).

[35] Giorgio Brida, M. V. Chekhova, G. A. Fornaro, Marco Genovese, E. D. Lopaeva, and I. R. Berchera, Systematic analysis of signal-to-noise ratio in bipartite ghost imaging with classical and quantum light, Phys. Rev. A **83**, 063807 (2011).